Computational Method for Bearing Surface Wear Prediction in Total Hip Replacements

Shawn Toh Ming Song[1,*], Ariyan Ashkanfar[1], Russell English[1], Glynn Rothwell[1]

[1]School of Engineering, Liverpool John Moores University, Byrom Street, Liverpool, UK, L3 3AF

Abstract

Total hip replacement (THR) is a revolutionary treatment when a hip joint becomes severely damaged. Wear is known as one of the main reasons for THR failure. Current experimental techniques to investigate the wear at the bearing surfaces of THRs are time-consuming, complicated and expensive. In this study, an in-house fretting wear algorithm has been further developed to investigate the wear damage that occurs on bearing surfaces of THRs and its consequence on the longevity of the implants. A 3D finite element model has been created with a 36mm diameter Cobalt-Chromium femoral head and a 4mm thick cross-linked polyethylene bearing liner. A gait loading cycle was used to simulate walking for up to 5 million cycles (Mc). The wear algorithm extracts relative displacements and contact shear stresses from the finite element package to predict the linear and volumetric wear rates. This method is shown to have modelled the evolution of wear effectively and found it to be similar to those from experimental analyses. The linear and volumetric wear per million cycles predicted in this study were 0.0375mm/Mc and 33.6mm^3/Mc which are comparable to those measured in-vivo THRs. The wear patterns obtained from this study are also comparable to the wear patterns shown on available conventional polyethylene liners. This method can be used to further aid in the design and clinical technique to reduce wear rate in THRs.

Keywords: Wear modelling, Total Hip Replacement, Hip joint prosthesis, Finite Element Modelling, polyethylene wear.

1. Introduction

A hip joint is one of the most important joints in our body. It bears our body weight in static and dynamic postures and plays an important role in retaining body balance; however, it may lose its functionality due to diseases such as osteoarthritis which causes pain and also in extreme cases, loss of mobility (Holcomb, Miller et al. 2012, Kumar, Bloch et al. 2017). When the joint has been severely damaged and physiotherapy, steroid injections or other treatments have not helped to improve mobility, the damaged joint may be removed and replaced with a prosthesis. According to the NJR's report in 2019, 82.6% of patients who received a total hip replacement (THR) had been suffering from osteoarthritis (NJR 2019). THR has become a revolutionary treatment (Nambiar, Jagani et al. 2017) over the last decades (Towheed and Hochberg 1996, Learmonth, Young et al. 2007, Ashman, Cruikshank et al. 2016). A THR usually consists of four parts, an acetabular cup, a bearing liner, a femoral head and a femoral stem (Figure 1). (Ali, Al-Hajjar et al. 2016, Varnum 2017) .

* Corresponding Author
E-mail addresses: s.m.toh@2016.ljmu.ac.uk , shawntoh15@gmail.com

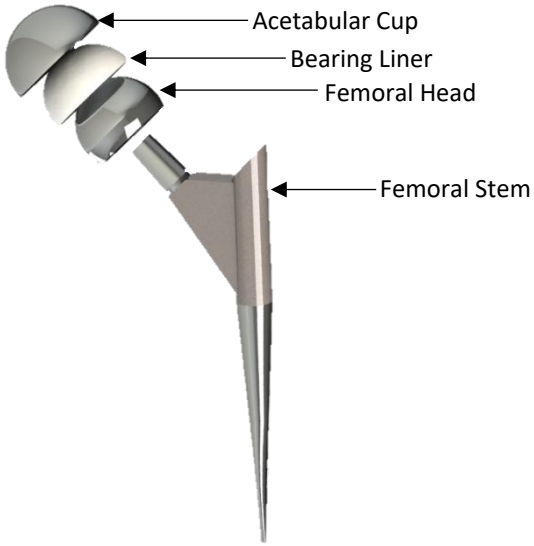

Figure 1: The four main parts of a total hip replacement (THR)

Data from the National Joint Registry (NJR) shows there were approximately 92,000 THR procedures performed in the United Kingdom using arthroplasty in 2018 with over a million THR's performed since 2003 (NJR 2019). Further statistics from the NJR in 2019, also shows that there is an average of 11.5% increase every year in the number of patients under 55 years old undergoing THR which suggests that more young active patients will undergo THR in the coming years. The longevity of these implants will need to be increased, as the current average lifespan of a THR implant is at 15 years (Evans, Evans et al. 2019). Furthermore, nearly 8% of cases had failed prematurely, less than 15 years in service, and needed a revision surgery (NJR 2019). Wear is one of the main reasons for premature failure in THRs (Karachalios, Komnos et al. 2018) and can cause a multitude of failure such as aseptic loosening, dislocation, infection or metallosis (Karachalios, Komnos et al. 2018, Neil G. Burke 2018, Sipek, Lyvers et al. 2018). Aseptic loosening accounts for approximately 45% of hip revisions (Buly, Huo et al. 1992, Neil G. Burke 2018, Sipek, Lyvers et al. 2018, NJR 2019).

Current experimental techniques to investigate the wear damage in THRs, such as radiography, tribo-testing, and hip joint simulators, are time-consuming, complicated and expensive (Hallan, Lie et al. 2006, Hua, Dou et al. 2019, Ramesh, van Kuilenburg et al. 2019). Computational analysis has several benefits when compared to experimental testing such as lower cost, lower run time, and having detailed solutions which can be an alternative to experimental techniques. With these added benefits, current computational analysis has led to the understanding of different design and material variations, (Shen, Lu et al. 2011, Ashkanfar, Langton et al. 2017, Gao, Hua et al. 2018, Ruggiero, Merola et al. 2018), manufacturing tolerances (Kluess, Martin et al. 2007, Ashkanfar, Langton et al. 2017, Affatato, Merola et al. 2018), and surgical techniques (English, Ashkanfar et al. 2016).

Recently, studies by Ruggiero, Sicilia et al. (2020) have used an in-silico approach to link experimental investigations to computational investigation to predict wear in the implant over millions of cycles. The main purpose of their study was to propose a wear prediction approach which would reproduce the classical in-vitro wear testing of total hip replacements accounting for unsteady synovial lubrication effects between the femoral head and the acetabular liner (Ruggiero and Sicilia 2020, Ruggiero, Sicilia et al. 2020). Understanding the wear pattern, damage and the wear

rates are crucial to identify the different key factors in prosthesis design, materials, tolerances and surgical methods which would minimise the wear rates and increase overall longevity.

Previously, an in-house fretting wear algorithm (English, Ashkanfar et al. 2015) was developed using a 3D finite element model and a Python script within the Abaqus environment. The algorithm has led to the further understanding of different design and material variations (Ashkanfar, Langton et al. 2017), manufacturing tolerances (Ashkanfar, Langton et al. 2017) and surgical techniques (English, Ashkanfar et al. 2016). The fretting wear algorithm was only able to predict wear due to micromotion at the taper junction of the THRs. In this study, a new wear algorithm has been developed to predict wear at the bearing surfaces for the larger movement of the femoral head.

2. Methodology

2.1. Finite element model

A model of the acetabular cup and femoral head with a liner insert was created in the finite element package (ABAQUS 2019) (Figure 2). In this model, the acetabular cup has a 4mm thick liner with a 3mm thick metal backing (Figure 2b) (Shen, Lu et al. 2011). The materials used in this analysis are Cobalt-Chromium (CoCr) for both the femoral head and acetabular cup and cross-linked polyethylene (XLPE) for the liner. XLPE has been widely used since the 2000s for its low wear by improving wear resistance and oxidative degradation while maintaining its' mechanical properties (Affatato, Ruggiero et al. 2018, Hu and Yoon 2018, Carli, Patel et al. 2020). The material properties are listed in Table 1 (Innocenti, Labey et al. 2014). The cup and head were meshed in preparation for analysis using the eight-node bilinear hexahedral reduced integration elements (C3D8R).

Table 1: Material Properties for THR

Material	Young's Modulus (GPa)	Density (kg/m^3)	Poisson's ration
CoCr	210	7800	0.3
XLPE	1	963	0.4

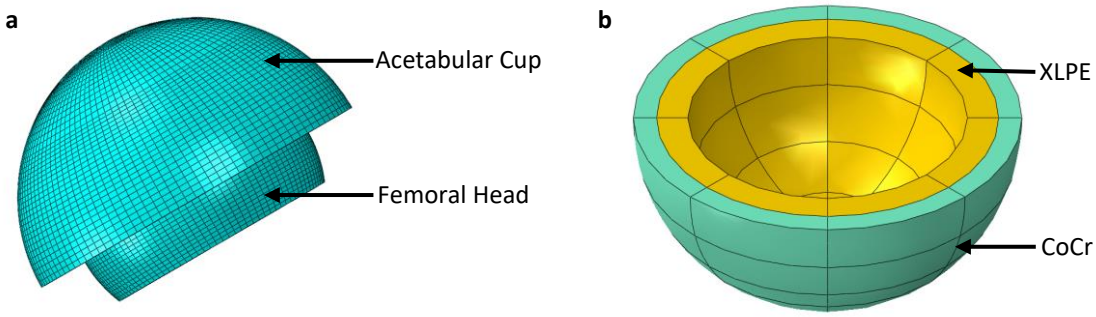

Figure 2: FE Model (a) Mesh of the FE model, (b) Partitions showing material assignments

To replicate a walking cycle, the rotations and loadings occurring on a typical hip joint were applied onto the model (Figure 3a). The acetabular cup was fixed on its outer surface whereas the femoral head was free to rotate based on the rotation and loading cycles specified. The walking loads and rotations (following their amplitude (Figure 4)) are both applied to the centre of the femoral head (Figure 3b, Figure 3c). These conditions simulate the acetabular cup as being cemented into the hip while the femoral head transfers the walking and rotation loads onto the inner surface of the acetabular cup. A friction coefficient of 0.11 (Wang, Ge et al. 2010) has been applied between the contacting surfaces using the penalty method in Abaqus.

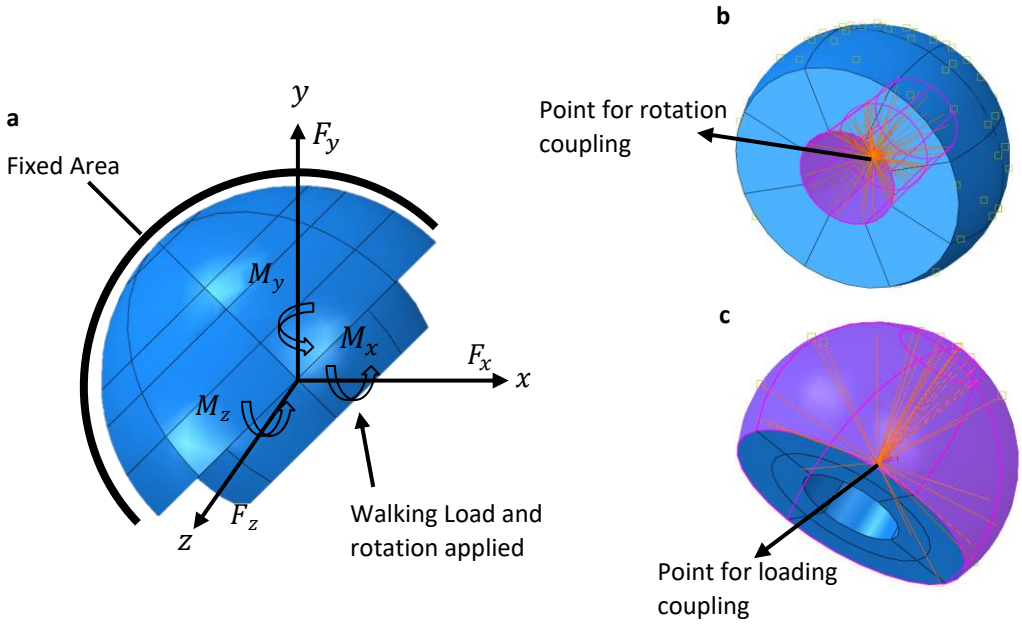

Figure 3: FE model: (a) showing boundary conditions on FE model, (b) area of rotation boundary applied, c) area of loading boundary applied

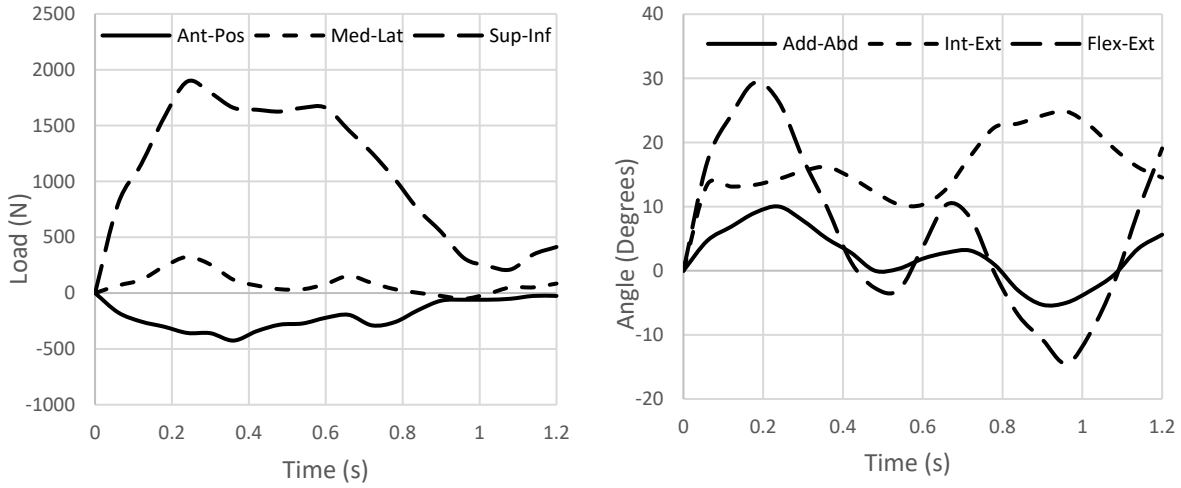

Figure 4: (a) Time variant loading cycle, (b) Time variant rotation walking gait cycle

2.2. Computational wear analysis

There are two main types of wear law, 'Archard's' and the 'Dissipated Energy' wear law (Zmitrowicz 2006, Abdo 2015). The Dissipated Energy wear law is used throughout this study as it predicts wear across a wider range of motion with a greater range of application than Archard's wear law (Fouvry, Liskiewicz et al. 2003, Abdo 2015). As elaborated previously by English, Ashkanfar et al. (2015), the wear depth (W_d) can be calculated using Eq. (1), where α is the energy wear coefficient, τ is the contact shear stress and *s* is the relative displacement between bearing surfaces.

$$W_d = \alpha \tau s \quad (1)$$

As the wear analysis would need to be performed for over millions of cycles, a scaling factor (β) needs to be introduced to make the execution of the analysis achievable in acceptable time. The scaling factor is used to multiply the wear calculated after a single analysis (one walking step) so as to create a wear value that can be used to modify the surface geometry by a suitable amount to

facilitate acceptable run times. The scaling factor used can vary across a large range (25,000 to 2 million). A large scaling factor would result in a faster computational run time but may affect the accuracy of the results. A small scaling factor would increase the computational run time but should provide a greater accuracy of results. Hence, the scaling factor needs to be optimised to ensure the accuracy of the results within an acceptable time frame. The wear for a single cycle of loading of a node can be calculated using Eq. (2), where τ_i and s_i are the surface contact shear stress and relative displacement respectively, at each time interval.

$$W_c = \beta \sum_{i}^{n} \alpha \, \tau_i s_i \tag{2}$$

The calculation of wear at the contact surfaces requires creating sets of "node pairs". The pairing is achieved by taking a node at the surface with the coarser mesh (Surface A) and determining which nodes are closest on the opposing surface (Surface B). In the previously developed fretting wear algorithm (English, Ashkanfar et al. 2015), as fretting wear does not involve any large displacements, a single node-to-node pairing method was sufficient to ensure that all the nodes would have wear depth applied. For the larger relative displacement, in this study, a node from 'Surface A' needs to be paired to a cloud of nodes on 'Surface B' due to different mesh densities on the surfaces. This will avoid any nodes on 'Surface B' to be left unpaired which may cause wear to not be applied at the node and subsequently cause sharp points in the geometry of the model. This has been optimised for each node from 'Surface A' to be paired to three to nine nodes on 'Surface B' (Figure 5). This depends on the difference in the mesh density on the coupling surfaces. The pairing procedure needs to be undertaken at each time interval of the walking cycle. The contact stress and relative displacement are extracted for all paired nodes at each time interval as illustrated in Figure 6.

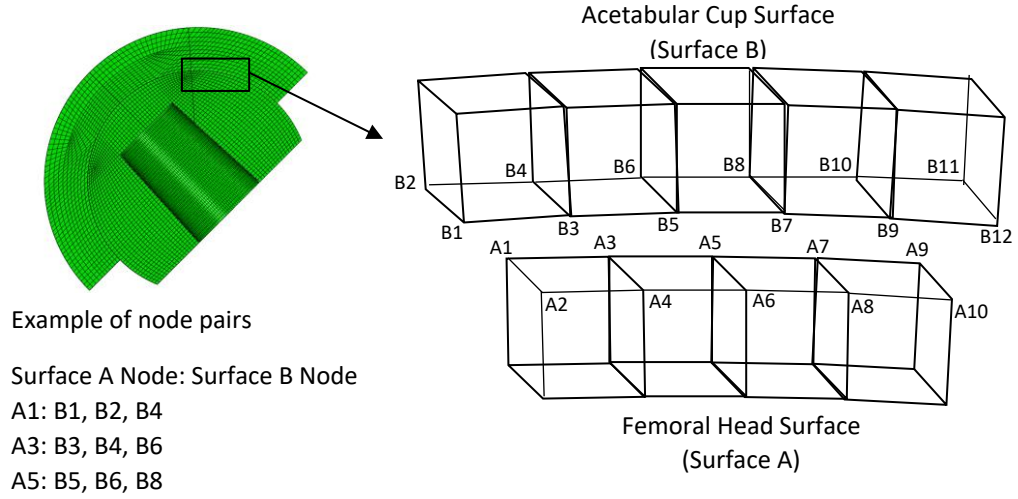

Figure 5: Node pairs diagram

Using Eq.(2), the wear depth for each set of paired nodes is calculated using an energy wear coefficient of $5.32(10^{-10})mm^3/Nmm$ (Matsoukas, Willing et al. 2009). A fraction of the wear depth calculated for each paired node is used to update the nodal coordinates. This fraction depends on the contact surface interaction properties of the materials in contact. The algorithm applies a fraction of the wear depth calculated on each contacting surface to each paired node. The wear fraction introduced is 0.99:0.01 for the interaction of XLPE with CoCr respectively (Anissian, Stark et al. 1999). Although the wear present in the CoCr is relatively small compared to XLPE, small amounts

of metal present in the body can lead to a metallosis. The wear fraction is used to highlight the amount of metal particles that would be released into the body.

To be able to translate wear depth into normal coordinates to update the geometry, the normal direction vectors of the nodes are obtained from the initial position of the model. The geometry is then updated based on the defined coordinates and a new input file is generated. The analysis is then continued until the number of cycles has been reached.

The scaling factor (β) used in the analysis has a great impact on computational time and wear accuracy. A larger scaling factor would result in a quicker analysis but may greatly impact the accuracy of the results. A smaller scaling factor would increase the computational effort. An optimum scaling factor of $\beta = 10^5$ was used in this study as previously investigated by (English, Ashkanfar et al. 2015).

The method to calculate the wear depth for hundreds of thousands of paired nodes needs to be automated. As such a Python script has been written within the Python Development Environment (PDE) in Abaqus to automate the procedure. An outline of the python script is shown in Figure 6. The python script is then converted into an Abaqus plug-in. Although the methodology here presented is using the 'Dissipated Energy' wear law, the algorithm can utilise both 'Archard' and 'Dissipated Energy' wear laws for calculations.

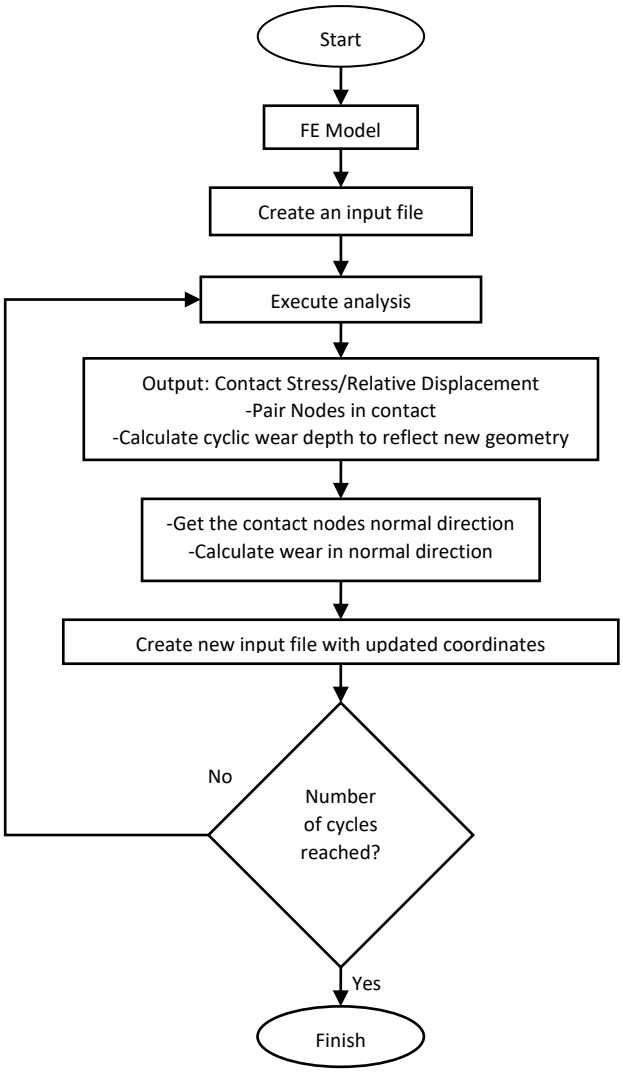

158

159 *Figure 6: Flowchart outlining python script*

160

161 The graphical user interface of the current wear algorithm is shown in Figure 7. All the necessary
162 variable inputs are taken from the user such as the wear coefficient (α), wear fraction, wear
163 equation to be used, the total number of updates and scaling factor. In addition to calculating the
164 wear depth, the volumetric wear can also be determined with the algorithm by extracting the
165 reduction of element volume for all elements throughout the entire part and calculated at each
166 defined time interval.

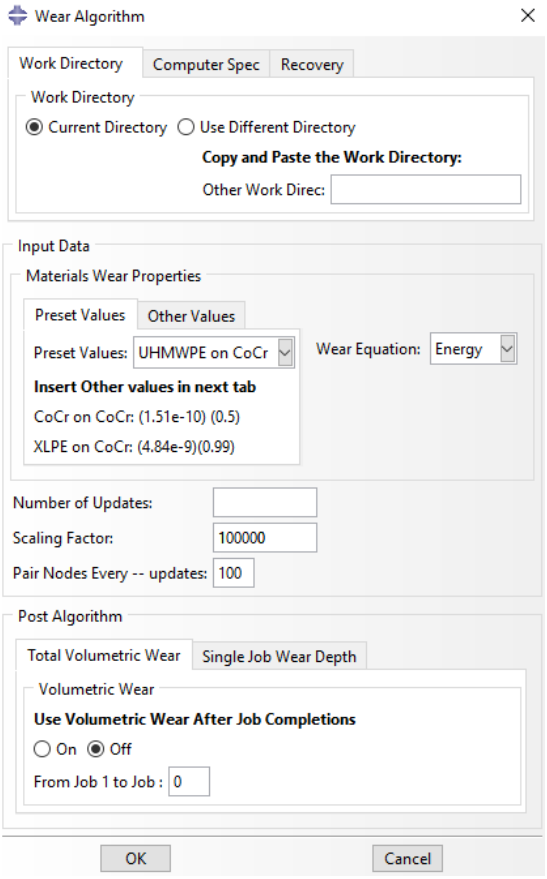

Figure 7: Graphical user interface of the wear algorithm

All analyses were executed on a 64-bit Windows 10 professional operating system with a four-core processor Intel central processing unit platform at 3.8 GHz which had a total run time of 850 hours.

3. Results

3.1. Variation of contact shear and relative displacement during a gait cycle.

Figure 8 shows the contact shear stress (CSHEAR), distributed on the femoral head, and relative displacement (CSLIP) on the bearing liner. It is noticeable that at each time interval, the CSHEAR and CSLIP at each point of the contact bearing surfaces are similar. The maximum CSHEAR is 0.352MPa which occurs at 0.60s while the maximum relative displacement of 10.9mm occurs at 0.24s over the walking cycle.

As explained earlier, the nodes in contact are paired at each time interval of the analysis. For each set of paired nodes, the CSLIP (Figure 8a) and CSHEAR (Figure 8b) were extracted. These values are then used to calculate the wear depth using Eq. (2). The wear depth distribution after using a scaling factor of 100,000 is shown in Figure 8c. As expected, due to the wear fraction, the highest wear depth occurs on the bearing liner with a wear depth of 4.25µm and the maximum wear depth on the femoral head is 0.0460µm which is around 99 times lower.

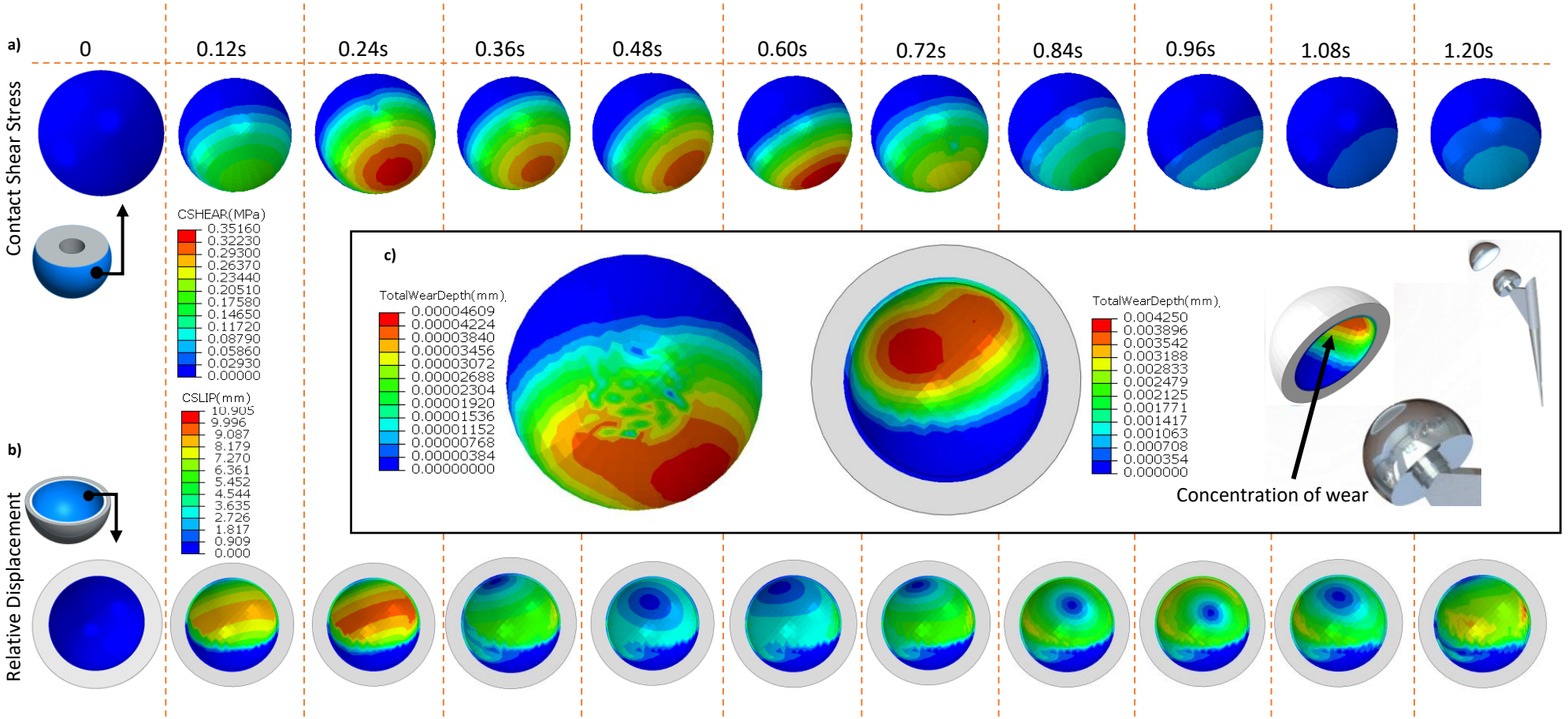

Figure 8: a) Variation of shear stresses, b) relative displacement during a walking cycle and the wear from the first 10,000 cycles, c) Wear depth values at the end of 100,000 cycles

3.2. Predicted wear damage over 5 million cycles

The same procedure as explained in 3.1 has been carried out to complete up to 5 million cycles and the evolution of wear is shown in Figure 9 at every million cycles. The maximum wear depth value reaches 192.5µm and 2.20µm after 5 million cycles for the bearing liner and femoral head respectively (Figure 9a, Figure 9b). It can be seen from Figure 9 that most of the wear occurs at a relatively small area.

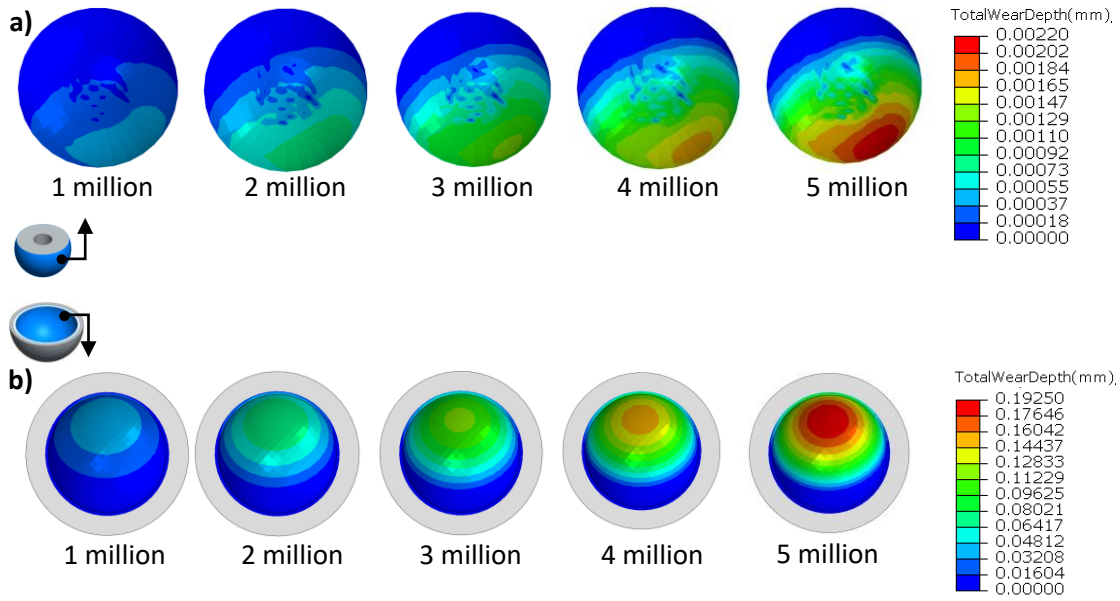

Figure 9: Variation in wear depth over 5 million walking cycles

3.3. Volumetric wear and linear wear of XLPE liner

The volumetric wear was determined at each 1 million cycles as the solution progressed based on the reduction of element volume for all the elements of the different parts. As can be expected, the material loss from the surfaces increases over the 5 million load cycles as shown in Figure 10a. The cumulative volumetric loss at the end of 5 million cycles is 169.2mm^3 and 1.75mm^3 for the XLPE bearing liner and CoCr femoral head due to the material interaction properties. The total material loss from both bearing surfaces after 5 million load cycles is 170.96mm^3. The volumetric wear rate at each million load cycle remains similar throughout the analysis between 33.6mm^3/Mc to 34.1mm^3/Mc and 0.337mm^3/Mc to 0.362mm^3/Mc for the bearing liner and femoral head respectively (Figure 10b). This shows that the volumetric wear is increasing linearly throughout the analysis.

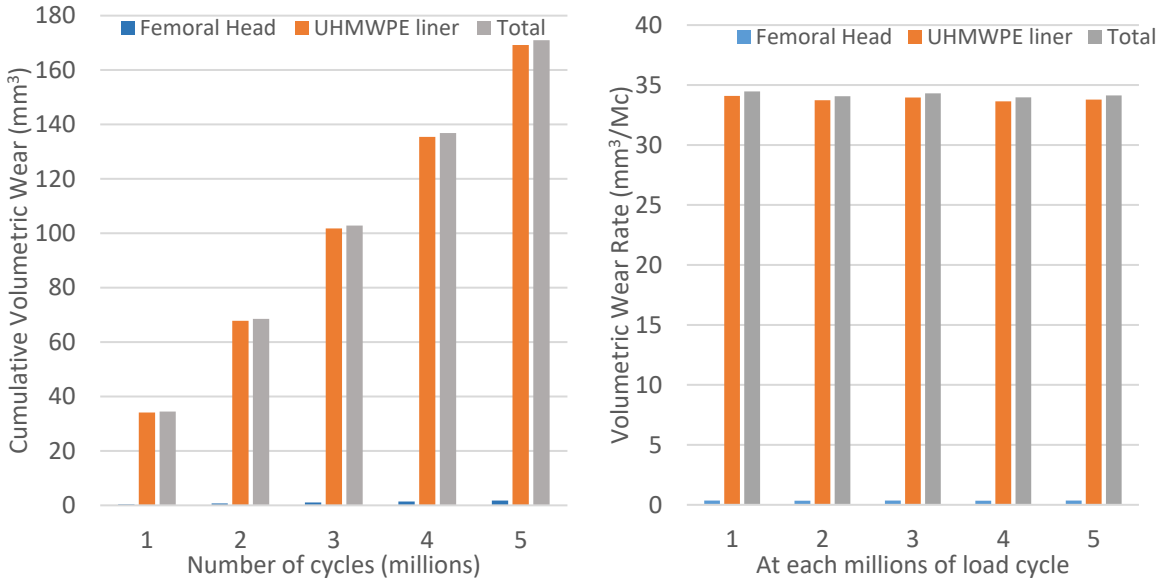

Figure 10: Variation in a) cumulative volumetric wear, b) volumetric wear rate with respect to n^{th} million cycles

The maximum linear wear was determined from the largest wear depth at the XLPE liner at each 0.5 million cycles (Figure 11). The maximum linear wear is shown to have a linear increase with a maximum of 0.192mm at 5 million cycles. The linear wear rate was initially higher for the first million load cycles at 0.0418mm/Mc and then decreases to about 0.0375 mm/Mc subsequently. The higher initial linear wear rate of 0.0418mm/Mc in the first million cycle (Figure 11b) may be due to an initial period of material deformation (bedding-in) and then steady-state wear which would continue after the first million cycle (A., E. et al. 2017).

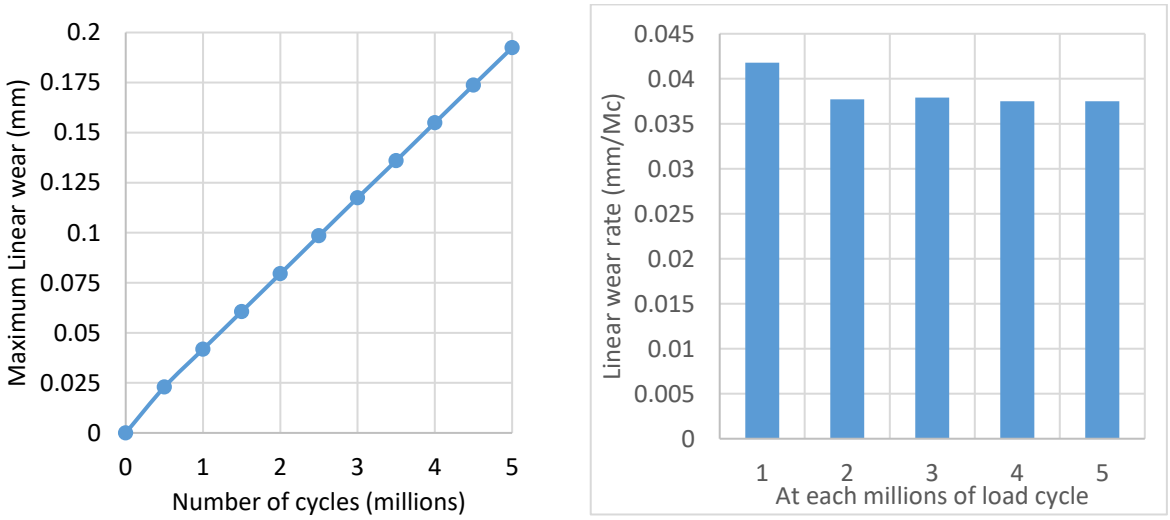

Figure 11: a) Maximum linear wear of XLPE liner at every million cycles, b) linear wear rate at each million of load cycles

4. Discussion

The scaling factor used in the analysis has a major impact on the solution time, wear evolution, and solution accuracy. Figure 12 shows the total cumulative wear and the wear that is applied at 2 million cycles using different scaling factors of 25,000, 50,000 and 100,000. Although the total cumulative wear at 2 million cycles remains similar, the wear that is being applied to the geometry is not smoothly distributed (Figure 12). As the analysis progresses, this will cause a sharp increase in wear depth at a certain contact area on the surfaces which would then lead to inconsistencies on the

wear pattern. To mitigate this effect and to reduce the computational time, a node wear smoothing feature has been developed in the wear algorithm. In this node smoothing feature, the wear applied to each node is checked with a cloud of surrounding nodes to ensure that the wear distribution is applied smoothly throughout the analysis.

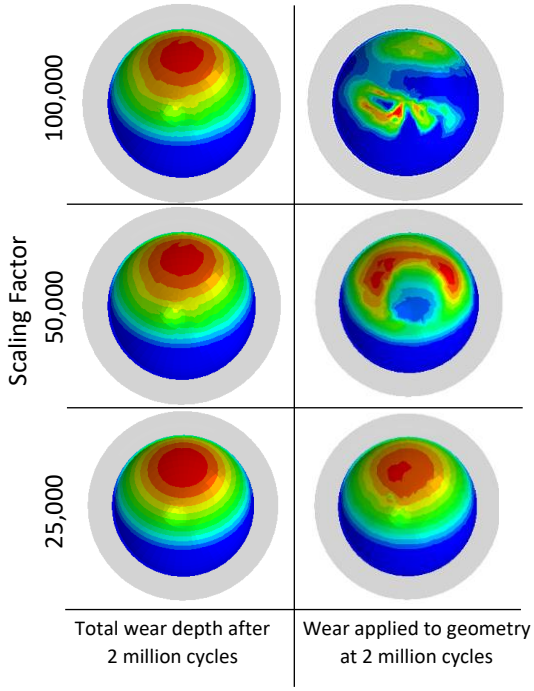

Figure 12: Effect of scaling factor on the wear occurring in the analysis

The maximum contact pressure variation over the first gait cycle is shown to be 3.21MPa (Figure 13a). At the end of 5 million cycles, the variation in contact pressure remains similar to the variation at the first gait cycle. These results are comparable to studies performed by Yoshida, Faust et al. (2006) and Saikko (2020). For a peak load of 2.5kN, Yoshida reported a maximum contact pressure of 3.2MPa while Saikko reported a maximum contact pressure of 3MPa.

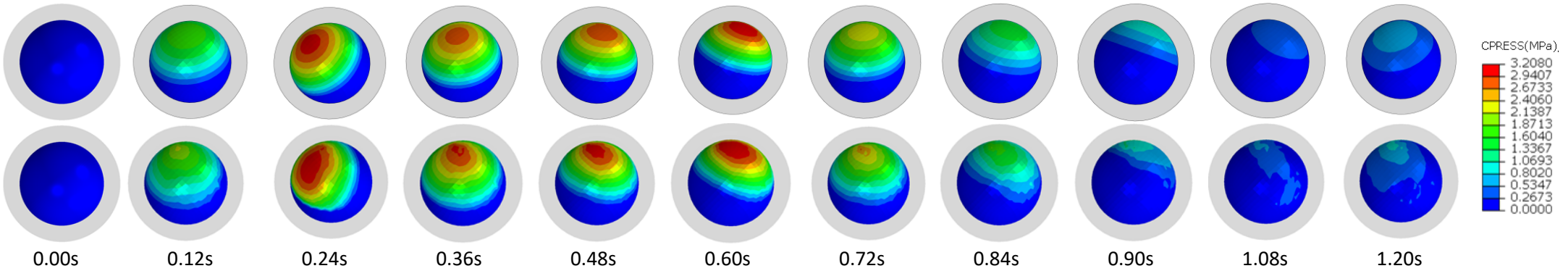

Figure 13: Variation of contact pressure (CPRESS) a) at the first gait cycle, b) at the end of 5 million cycles

The linear and volumetric wear rates shown in this study are comparable to several studies with XLPE in the literature (see Table 2). A., E. et al. (2017) and Haw, Battenberg et al. (2017) analysed a total of 32 and 48 primary total hip arthroplasties respectively with a 36mm CoCr femoral head size coupled with XLPE liners on serial radiographs. A., E. et al. (2017) showed a mean linear and volumetric wear rate of 0.07mm/yr and 29.29mm^3/yr while Haw, Battenberg et al. (2017) showed a mean linear and volumetric wear rate of 0.052mm/yr and 33.09mm^3/yr. Khoshbin, Wu et al. (2020) analysed a total of 40 primary THR of XLPE liners with CoCr femoral heads using radiography. The results obtained showed a mean linear wear rate of 0.0387mm/yr and 31.51mm^3/yr.

The range of linear and volumetric wear rate for the XLPE liners coupled with a 36mm CoCr femoral head reported in the above studies (A., E. et al. 2017, Haw, Battenberg et al. 2017, Khoshbin, Wu et al. 2020) was between 0.039 - 0.07mm/yr and 29.29 - 33.09mm^3/yr. The number of steps walked by a patient per year, undoubtedly influences the wear rate per year however by considering an average of 1 million walking steps per year (Schmalzried, Szuszczewicz et al. 1998), the linear and volumetric wear rate shown in our study (0.0375mm/yr and 33.8mm^3/yr) are comparable to those found in the above literature (see Table 2Figure 2). It is noticeable that if a patient walks more than the assumed 1 million cycles per year, it will only hasten the wear and not affect the wear rate per million cycles. There are many factors which can contribute to the wear damage, such as variable wear and friction coefficients, surface roughness, manufacturing tolerances, and the patient's activity level, weight, and implant design.

Table 2: Linear and volumetric wear rates of XLPE and UHMWPE in literature.

Material	Literature	Method of wear retrieval	Linear Wear rate (mm/yr)	Volumetric Wear rate (mm^3/yr)
XLPE	A., E. et al. (2017)	Radiography	0.07	29.29
	Haw, Battenberg et al. (2017)	Radiography	0.052	33.09
	Khoshbin, Wu et al. (2020)	Retrieved THR	0.0387	31.51
	Range	-	0.039 – 0.07	29.3 – 33.1
	Current study	**FEA**	**0.0375**	**33.8**
UHMWPE	Ali, Al-Hajjar et al. (2016)	Hip Simulator	0.24	12.2
	Trommer, Maru et al. (2015)	Hip Simulator	0.8	56
	Callaghan, Pedersen et al. (2003)	Clinical database	0.08 – 0.12	32.71 – 89.27
	Fialho, Fernandes et al. (2007)	Computational Method	0.09	18
	Literature range	-	0.08 – 0.8	12.2 – 89.3

As XLPE liners are a relatively new material (around 15 years) compared to conventional ultra-high-molecular-weight polyethylene (UHMWPE) (around 50 years), many of the primary THR conducted are still currently in service and the investigation on the wear rate is mainly based on radiography as shown in the above literature. Radiography is unable to show the wear pattern on the bearing surface which is paramount to understanding the evolution of wear. The wear algorithm presented in this study can show the wear pattern and highlight areas of concern.

To further understand and compare the wear evolution, the wear patterns of conventional UHMWPE were compared with the results shown in this study (see Table 2). A study by Ali, Al-Hajjar et al. (2016) and Trommer, Maru et al. (2015) which both used a commercial hip simulator to evaluate the wear at 5 million load cycles showed a linear and volumetric wear rate of 0.24mm/yr and 12.2mm^3/yr for a 36mm CoCr femoral head and 0.8mm/yr and 56mm^3/yr for a 28mm CoCr femoral head. Callaghan, Pedersen et al. (2003) used a clinical database of more than 4000 primary THRs with 22mm and 28mm femoral head sizes implanted by a surgeon to evaluate the wear mechanism between 5 and 22 years. The range of linear and volumetric wear presented was 0.08 -

0.12mm/yr and 32.71 - 89.27mm^3/yr respectively. Fialho, Fernandes et al. (2007) used a computational method to predict the extent of wear damage for a 28mm CoCr head size at 1 million load cycles. The study showed a linear and volumetric wear rate of 0.09mm/Mc and 18mm^3/Mc.

The range of linear and volumetric wear presented for conventional UHMWPE liners in the above studies (Callaghan, Pedersen et al. 2003, Fialho, Fernandes et al. 2007, Trommer, Maru et al. 2015, Ali, Al-Hajjar et al. 2016) was between 0.08 – 0.24mm/Mc and 12.2 – 89.27mm^3/yr respectively. Although the wear patterns in our study are comparable to the wear pattern shown in conventional UHMWPE, the linear and volumetric wear rates of conventional UHMWPE are higher than the values shown in XLPE as the overall amount of wear of XLPE may be up to 40% less (Ali, Al-Hajjar et al. 2016) than conventional UHMWPE (see Table 2).

Although in this study we have used zero tolerances between the femoral head and bearing liner, defining tolerances for manufacturing is crucial. The tolerances may also translate into bearing surface clearances which will affect the outcome of wear and implant survivability. Surface roughness may also influence wear. There have been studies which incorporate surface roughness into the wear coefficient to simulate the actual wear (Pietrabissa, Raimondi et al. 1998, Raimondi, Santambrogio et al. 2001). The algorithm developed in this study can be used to perform parametric studies to propose the optimum tolerances for manufacturing and surface roughness.

A fixed friction coefficient and wear coefficient has been used in this study; however, they can be continuously changed over the implant's lifetime due to the changes in surface roughness, lubrication and wear debris. The algorithm developed in this study can investigate the effect of different friction and wear coefficients to improve the design and material characteristics of the implant.

5. Conclusion

The combination of using a wear algorithm written in the PDE and a 3D FE model presented in this study can be used to predict the extent of bearing surface wear damage for millions of load cycles. The algorithm developed can be applied to clinical practice such as determining appropriate bearing size, bearing liner thickness, implantation angle, and to improve the design of the prosthesis to increase its longevity.

The methodology demonstrates that a dynamic implicit analysis can model the gait cycle effectively. The total dissipated energy wear law and the FE model described can predict wear patterns, linear and volumetric wear rates when compared to typically observed wear patterns from UHMWPE retrievals and XLPE in-vivo wear rates. These results have been validated with literature and show promise in predicting the evolution of wear and can be used to investigate different parameters such as body weight, material properties, different implant size and design, manufacturing tolerances and different surgical techniques.

The accurate and smooth evolution of wear across the bearing surface are influenced by the scaling factor and mesh size used. Using a courser mesh density and a large scaling factor would reduce the computational time but will affect the accuracy of the results. A smaller scaling factor (Figure 12) would ensure that the wear is evenly distributed and will avoid cyclic wear 'hotspots' being overly exaggerated. A fine mesh and a small scaling factor can facilitate an accurate and smooth development of wear but with the cost of a much-increased computational time. To help reduce the computational time, a node smoothing feature was developed to be used so there is no sudden exaggeration in the node wear. As such, a balance of mesh density and the scaling factor is needed to ensure accurate results within a reasonable time. For example, the model presented in this study

has utilised a scaling factor of 100,000 coupled with the node smoothing feature was found to provide a smooth wear evolution.

The wear methodology can be utilised generically in the analysis of other prosthetic devices such as knee and shoulder implants. Also, the method can be generalised to involve parts in contact subject to cyclic loadings.

Acknowledgement

This work is funded by the School of Engineering, Liverpool John Moores University, Liverpool, UK.

References

A., A., W. S. E., K. A., H. N., B. E., S. E. H. and W. J. P. (2017). "Ten-year follow-up study of three alternative bearing surfaces used in total hip arthroplasty in young patients." The Bone & Joint Journal **99-B**(12): 1590-1595.

Abdo, J. (2015). "Materials Sliding Wear Model Based on Energy Dissipation." Mechanics of Advanced Materials and Structures **22**(4): 298-304.

Affatato, S., M. Merola and A. Ruggiero (2018). "Development of a Novel in Silico Model to Investigate the Influence of Radial Clearance on the Acetabular Cup Contact Pressure in Hip Implants." Materials **11**(8): 1282.

Affatato, S., A. Ruggiero, S. A. Jaber, M. Merola and P. Bracco (2018). "Wear behaviours and oxidation effects on different uhmwpe acetabular cups using a hip joint simulator." Materials **11**(3): 433.

Ali, M., M. Al-Hajjar and L. M. Jennings (2016). 31 - Tribology of UHMWPE in the Hip. UHMWPE Biomaterials Handbook (Third Edition). S. M. Kurtz. Oxford, William Andrew Publishing**:** 579-598.

Ali, M., M. Al-Hajjar, S. Partridge, S. Williams, J. Fisher and L. M. Jennings (2016). "Influence of hip joint simulator design and mechanics on the wear and creep of metal-on-polyethylene bearings." Proceedings of the Institution of Mechanical Engineers, Part H: Journal of Engineering in Medicine **230**(5): 389-397.

Anissian, L., A. Stark, K. Sorensen, A. Gustafson, B. Downs, V. Good and I. Clarke (1999). HIP-SIMULATOR WEAR COMPARISONS OF COCR/COCR VERSUS COCR/PE THR AT 10 MILLION CYCLES. Proceedings of the Annual Meeting of the Orthopaedic Research Society, Anaheim, California.

Ashkanfar, A., D. J. Langton and T. J. Joyce (2017). "Does a micro-grooved trunnion stem surface finish improve fixation and reduce fretting wear at the taper junction of total hip replacements? A finite element evaluation." Journal of Biomechanics **63**: 47-54.

Ashkanfar, A., D. J. Langton and T. J. Joyce (2017). "A large taper mismatch is one of the key factors behind high wear rates and failure at the taper junction of total hip replacements: A finite element wear analysis." Journal of the mechanical behavior of biomedical materials **69**: 257-266.

Ashman, B., D. Cruikshank and M. Moran (2016). "Total hip replacement: Relieving pain and restoring function." British Columbia Medical Journal **58**(9): 505-513.

Buly, R. L., M. H. Huo, E. Salvati, W. Brien and M. Bansal (1992). "Titanium wear debris in failed cemented total hip arthroplasty: An analysis of 71 cases." The Journal of Arthroplasty **7**(3): 315-323.

Callaghan, J. J., D. R. Pedersen, R. C. Johnston and T. D. Brown (2003). "Clinical biomechanics of wear in total hip arthroplasty." The Iowa orthopaedic journal **23**: 1.

Carli, A. V., A. R. Patel, M. B. Cross, D. J. Mayman, K. M. Carroll, P. M. Pellicci and S. A. Jerabek (2020). "Long-term performance of oxidized zirconium on conventional and highly cross-linked polyethylene in total hip arthroplasty." SICOT-J **6**.

English, R., A. Ashkanfar and G. Rothwell (2015). "A computational approach to fretting wear prediction at the head–stem taper junction of total hip replacements." Wear **338-339**: 210-220.

English, R., A. Ashkanfar and G. Rothwell (2016). "The effect of different assembly loads on taper junction fretting wear in total hip replacements." Tribology International **95**: 199-210.

Evans, J. T., J. P. Evans, R. W. Walker, A. W. Blom, M. R. Whitehouse and A. Sayers (2019). "How long does a hip replacement last? A systematic review and meta-analysis of case series and national registry reports with more than 15 years of follow-up." The Lancet **393**(10172): 647-654.

Fialho, J. C., P. R. Fernandes, L. Eça and J. Folgado (2007). "Computational hip joint simulator for wear and heat generation." Journal of Biomechanics **40**(11): 2358-2366.

Fouvry, S., T. Liskiewicz, P. Kapsa, S. Hannel and E. Sauger (2003). "An energy description of wear mechanisms and its applications to oscillating sliding contacts." Wear **255**(1): 287-298.

Gao, L., Z. Hua and R. Hewson (2018). "Can a “pre-worn” bearing surface geometry reduce the wear of metal-on-metal hip replacements? – A numerical wear simulation study." Wear **406-407**: 13-21.

Hallan, G., S. A. Lie and L. I. Havelin (2006). "High wear rates and extensive osteolysis in 3 types of uncemented total hip arthroplasty: A review of the PCA, the Harris Galante and the Profile/Tri-Lock

Plus arthroplasties with a minimum of 12 years median follow-up in 96 hips." Acta Orthopaedica **77**(4): 575-584.
Haw, J. G., A. K. Battenberg, D.-C. T. Huang and T. P. Schmalzried (2017). "Wear Rates of Larger-Diameter Cross-Linked Polyethylene at 5 to 13 Years: Does Liner Thickness or Component Position Matter?" The Journal of Arthroplasty **32**(4): 1381-1386.
Holcomb, W. R., M. G. Miller and M. D. Rubley (2012). "Importance of Comprehensive Hip Strengthening." Strength & Conditioning Journal **34**(1): 16-19.
Hu, C. Y. and T.-R. Yoon (2018). "Recent updates for biomaterials used in total hip arthroplasty." Biomaterials research **22**: 33-33.
Hua, Z., P. Dou, H. Jia, F. Tang, X. Wang, X. Xiong, L. Gao, X. Huang and Z. Jin (2019). "Wear Test Apparatus for Friction and Wear Evaluation Hip Prostheses." Frontiers in Mechanical Engineering **5**(12).
Innocenti, B., L. Labey, A. Kamali, W. Pascale and S. Pianigiani (2014). "Development and validation of a wear model to predict polyethylene wear in a total knee arthroplasty: a finite element analysis." Lubricants **2**(4): 193-205.
Karachalios, T., G. Komnos and A. Koutalos (2018). "Total hip arthroplasty: Survival and modes of failure." EFORT open reviews **3**(5): 232-239.
Khoshbin, A., J. Wu, S. Ward, L. T. Melo, E. H. Schemitsch, J. P. Waddell and A. Atrey (2020). "Wear Rates of XLPE Nearly 50% Lower Than Previously Thought After Adjusting for Initial Creep: An RCT Comparing 4 Bearing Combinations." JBJS Open Access **5**(2): e0066.
Kluess, D., H. Martin, W. Mittelmeier, K.-P. Schmitz and R. Bader (2007). "Influence of femoral head size on impingement, dislocation and stress distribution in total hip replacement." Medical Engineering & Physics **29**(4): 465-471.
Kumar, A., B. V. Bloch and C. Esler (2017). "Trends in Total Hip Arthroplasty in Young Patients - Results from a Regional Register." HIP International **27**(5): 443-448.
Learmonth, I. D., C. Young and C. Rorabeck (2007). "The operation of the century: total hip replacement." The Lancet **370**(9597): 1508-1519.
Matsoukas, G., R. Willing and I. Y. Kim (2009). "Total Hip Wear Assessment: A Comparison Between Computational and In Vitro Wear Assessment Techniques Using ISO 14242 Loading and Kinematics." Journal of Biomechanical Engineering **131**(4).
Nambiar, S. M., N. S. Jagani, L. Sharoff and J. J. D'souza (2017). "Total hip replacement the ideal joint for failed osteosynthesis of hip fractures." International Journal of Orthopaedics **3**(3): 667-672.
Neil G. Burke, J. P. G., Adrian J. Cassar-Gheiti, Fionnuala M. Walsh, James P. Cashman (2018). "Total hip replacement—the cause of failure in patients under 50 years old?" Ir J Med Sci (2019) 188: 879.
NJR (2019). National Joint Registry: National Joint Registry for England, Wales and Northern Ireland; 16th Annual Report, 2019.
Pietrabissa, R., M. Raimondi and E. Di Martino (1998). "Wear of polyethylene cups in total hip arthroplasty: a parametric mathematical model." Medical Engineering & Physics **20**(3): 199-210.
Raimondi, M. T., C. Santambrogio, R. Pietrabissa, F. Raffelini and L. Molfetta (2001). "Improved mathematical model of the wear of the cup articular surface in hip joint prostheses and comparison with retrieved components." Proceedings of the Institution of Mechanical Engineers, Part H: Journal of Engineering in Medicine **215**(4): 377-390.
Ramesh, V., J. van Kuilenburg and W. W. Wits (2019). "Experimental Analysis and Wear Prediction Model for Unfilled Polymer–Polymer Sliding Contacts." Tribology Transactions **62**(2): 176-188.
Ruggiero, A., M. Merola and S. Affatato (2018). "Finite Element Simulations of Hard-On-Soft Hip Joint Prosthesis Accounting for Dynamic Loads Calculated from a Musculoskeletal Model during Walking." Materials **11**(4): 574.
Ruggiero, A. and A. Sicilia (2020). "Lubrication modeling and wear calculation in artificial hip joint during the gait." Tribology International **142**: 105993.

Ruggiero, A., A. Sicilia and S. Affatato (2020). "In silico total hip replacement wear testing in the framework of ISO 14242-3 accounting for mixed elasto-hydrodynamic lubrication effects." Wear **460-461**: 203420.
Saikko, V. (2020). "Effect of inward-outward rotation on hip wear simulation." Journal of Biomechanics **101**: 109638.
Schmalzried, T. P., E. S. Szuszczewicz, M. R. Northfield, K. H. Akizuki, R. E. Frankel, G. Belcher and H. C. Amstutz (1998). "Quantitative assessment of walking activity after total hip or knee replacement." Journal of Bone and Joint Surgery - Series A **80**(1): 54-59.
Shen, F.-W., Z. Lu and H. A. McKellop (2011). "Wear versus thickness and other features of 5-Mrad crosslinked UHMWPE acetabular liners." Clinical Orthopaedics and Related Research® **469**(2): 395-404.
Sipek, K., M. Lyvers and M. Mathew (2018). "Failure Causes in Total Hip Replacements: A review." Austin J Orthopade & Rheumatol **5:1064**.
Towheed, T. E. and M. C. Hochberg (1996). "Health-related quality of life after total hip replacement." Seminars in Arthritis and Rheumatism **26**(1): 483-491.
Trommer, R. M., M. M. Maru, W. L. Oliveira Filho, V. P. S. Nykanen, C. P. Gouvea, B. S. Archanjo, E. H. Martins Ferreira, R. F. Silva and C. A. Achete (2015). "Multi-Scale Evaluation of Wear in UHMWPE-Metal Hip Implants Tested in a hip Joint Simulator." Biotribology **4**: 1-11.
Varnum, C. (2017). "Outcomes of different bearings in total hip arthroplasty - implant survival, revision causes, and patient-reported outcome." Dan Med J **64**(3).
Wang, S. B., S. R. Ge, H. T. Liu and X. L. Huang (2010). Wear behaviour and wear debris characterization of UHMWPE on alumina ceramic, stainless steel, CoCrMo and Ti6Al4V hip prostheses in a hip joint simulator. Journal of Biomimetics, Biomaterials and Tissue Engineering, Trans Tech Publ.
Yoshida, H., A. Faust, J. Wilckens, M. Kitagawa, J. Fetto and E. Y. S. Chao (2006). "Three-dimensional dynamic hip contact area and pressure distribution during activities of daily living." Journal of Biomechanics **39**(11): 1996-2004.
Zmitrowicz, A. (2006). "Wear patterns and laws of wear-a review." JOURNAL OF THEORETICAL AND APPLIED MECHANICS **44**: 219-253.